Chapter 1

Introduction

"Let noble thoughts come to us from all directions in the universe"

–Rigveda 1.89.1

The Sun, a big ball of fire that changes its color from dawn to dusk when viewed from the Earth, is the source of energy and life on the Earth. History shows a close relationship between human civilization and the Sun. In every ancient civilization, Sun is depicted as a god of superpowers. Sun has been mysterious from the past for humans. As human civilization has evolved, the understanding of the Sun has increased. Even in the 21^{st} century, a technological era, humans have not understood the Sun very well.

Understanding the Sun is important as it affects human life and the Earth not only as a source of energy that keeps the planet habitable but also in various ways. Highly explosive and energetic events like solar flares, coronal mass ejections (CMEs), etc. occur on the Sun and release large amounts of energy, magnetic fields, charged particles, and X-rays into the interplanetary medium. These events create space weather and affect the heliosphere and the global climate on Earth. These highly energetic charged particles and ions interact with the Earth's magnetic field and can be the cause of a geomagnetic disturbance in the Earth's magnetosphere and ionosphere. This geomagnetic disturbance affects the power

grids, telegraph systems, uninterrupted segments of the oil and natural gas pipelines, and navigation of airplanes. Furthermore, the charged particles and ions enter the Earth's atmosphere and collide with the atmospheric atoms and molecules and these atoms go into excited states and emit different beautiful colors of light which are visible in the polar region of the Earth and known as auroras. High solar activity also damages satellites in space and interrupts radio-wave propagation and navigation-system stability on the Earth. Astronauts living in space can suffer from the sun's radiation and due to this, they can also get serious diseases and death.

Thus Sun has a profound and interconnected relationship with the Earth and all its living beings, directly and indirectly. Indeed, the impact of the Sun extends far beyond the Earth, encompassing the entire solar system. The ultimate cause of all these severe events is the solar magnetic field. The strength of the Sun's magnetic field is commonly measured using the sunspot number, which is a way to quantify the number of sunspots observed on the solar surface. The sunspots are the seats of strong magnetic field $\sim (1000 - 3000)\ G$, and its number varies over time, which follows a well-known pattern of maxima and minima known as the solar cycle of about 11 years. However, in the 17th century, extremely low sunspot numbers were observed on the solar surface for about 70 years, known as the Maunder minimum. Several records indicate that in this extended period of low solar activity, several parts of Northern Europe went through an unusually cold temperature, and no aurorae were seen on the Earth.

As human civilization is advancing, we are becoming more and more technology-dependent and thus more vulnerable to solar activity. Hence, understanding solar magnetic field origin and its behavior is essential. Starting the exploration to know about the Sun's magnetic field, several crucial questions naturally emerge:

1) Origin of the Sun's magnetic field and its sustenance against the ohmic dissipation throughout its lifespan.

2) What is the underlying cause of the variability observed in the solar magnetic field, both long-term and short-term?

3) Can we develop the capability to predict future variations of the solar magnetic field, and if so, what are the fundamental physical processes that govern such predictions?

Discovering possible answers to these questions is my thesis objective. Uncovering answers to these questions will help us to understand the underlying fundamental physical process of magnetic field generation mechanism in the Sun and sun-like stars.

1.1 Solar Magnetism and Cycle

The Sun's magnetic field plays a key role in shaping its activity and influencing various phenomena occurring on its surface and outer atmosphere. The nature of the Sun's magnetic field is very complex and dynamic. The first indication of the solar magnetic field was measured by Hale (1908) using the Zeeman effect in sunspots which are the cooler and darker regions on the solar surface where the magnetic field is concentrated. The strength of these concentrated magnetic field is of the kilo Gauss order. The strong magnetic field of sunspots inhibits the convective motions that transport heat from the Sun's interior to its surface, and thus the region appears cooler and darker than its surroundings (about 1500 – 2000° C lower). Due to the strong magnetic field, sunspots exhibit complex structures. Figure 1.1 shows a few (typical) sunspots. The dark central region of a sunspot is known as the umbra where the magnetic field is strongest and approximately vertical, or normal, to the Sun's surface, while the lighter surrounding area is known as the penumbra. The penumbra consists of filamentary structures and is composed of magnetic field lines that are less concentrated than those in the umbra. Sunspots can vary in size, with giant sunspots being several times the diameter of Earth. The typical size of a fully evolved sunspot is about 10,000 km. The lifetime of a sunspot varies from hours to a few weeks, which

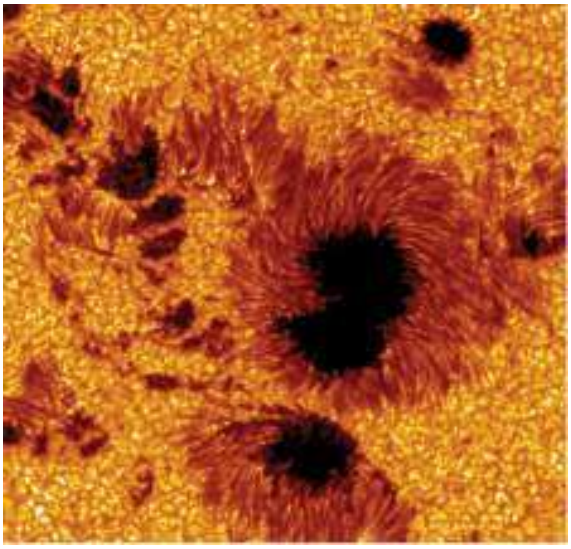

Fig. 1.1 Image of the group sunspots and surrounding granules on the solar surface for the active region(AR) 10030. The image was taken on 15 July 2002 by Swedish 1-m solar Telescope. The image has been colored yellow for aesthetic reasons. (*Image courtesy: Royal Swedish Academy of Sciences*).

depends on its size, magnetic complexity, and the overall level of solar activity (Bradshaw & Hartigan, 2014; Tlatov, 2023).

Furthermore, sunspots emerge in binary groups on the solar surface, and they are bipolar i.e., the preceding and following sunspots are opposite in polarity (Hale et al., 1919). Also, the corresponding spots of such groups are of opposite polarity in the Nothern and Southern hemispheres. Moreover, the spots of the present cycle are opposite in polarity to those of the last 11-year solar cycle. The sunspots predominantly manifest in an east-to-west direction, with a slight tilt relative to the Sun's equator. The tilt angle of sunspots is observed to increase statistically with the latitude, which is known as Joy's law (Hale et al., 1919). Furthermore, there is a considerable amount of scatter in the tilt angle around Joy's law (Howard, 1991; Jha et al., 2020; Sreedevi et al., 2023; Stenflo, 2012). Figure 1.2 shows the magnetograms of the Sun, which shows the regions of strong magnetic field that appeared as sunspots in the white light. We can see that the two opposite polarity

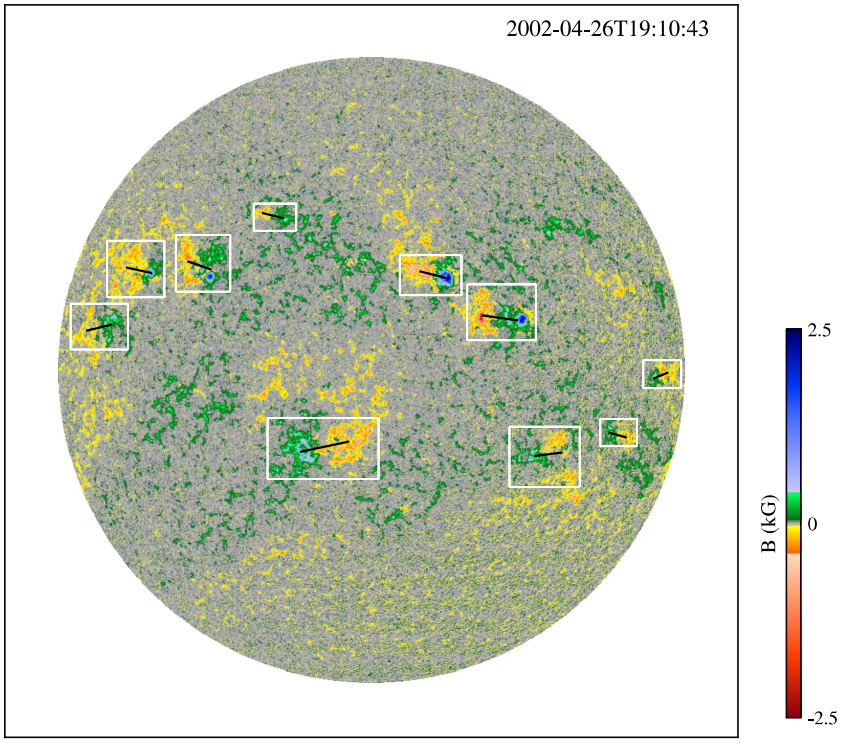

Fig. 1.2 Vertical flux density map, calculated from the MDI line-of-sight magnetogram recorded on 2002 April 26. The IDL program has identified 10 bipolar magnetic regions and enclosed them in rectangular boxes. The gray-scale cuts are set at +2.5 kG (blue) and −2.5 kG (red). (*Image courtesy: Sreedevi et al. (2023)).*

sunspots are located next to each other, and thus, sunspots are the structures of a general feature called bipolar magnetic regions (BMRs). We also note that the polarity orientation of BMR is opposite in the two hemispheres, and they are tilted with respect to the equator. Another feature of sunspots or BMRs is that they emerge below $\pm 40^{\circ}$ latitudes on the solar surface. As the solar cycle progresses, sunspot eruptions occur from mid to low latitudes (*Spörer*'s law) as seen in Figure 1.3.

Besides the sunspot's magnetic field, the polar field is another prominent large-scale magnetic field observed on the Sun. The concentration of this magnetic field is primarily observed at the heliographic poles of the Sun. Usually, the polar field is measured by taking the average value from 55° to the poles(Svalgaard et al., 1978), however, some

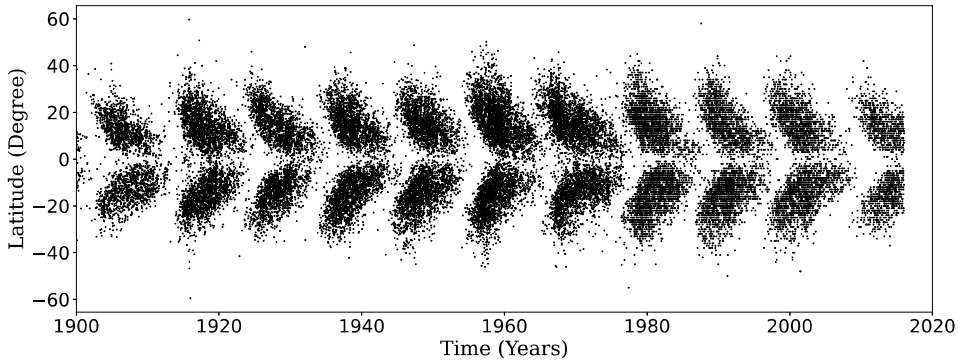

Fig. 1.3 Time-latitude distribution of the sunspots (butterfly diagram), showing the emergences below about $\pm 40^{\circ}$ latitudes. Note that in every cycle, the latitudes of sunspots drift toward the equator as the cycle progresses. (*Source: https://vizier.cfa.harvard.edu/*).

authors use different window; see Golubeva et al. (2023) for details. The polar field of the Sun has unipolar nature, unlike the sunspots. The magnetic field distribution has opposite polarity at the two poles of the Sun. The observed average field strength of the polar field is about 10 G which is very weak than the sunspot field strength ($\sim$ 3000 G). However, high-resolution observations revealed a unipolar but highly complex and non-uniform flux distribution, containing ubiquitous fields of greater strength (kG) Petrie (2015).

Unlike active region flux (mainly sunspots), most polar field lines do not connect back to the Sun. Therefore, they have a significant contribution to the interplanetary magnetic field. The open polar field lines form the polar coronal holes on the Sun and dominate in the solar corona. The Sun's polar field exhibits a periodic variation in its polarity similar to the solar cycle on average 11 years, around the time of solar maximum. It is worth noting that the reversal timing of the polar field in the Sun also varies from cycle to cycle. However, determination of the time of reversal with high accuracy is impossible due to poor observations of polar regions (Golubeva et al., 2023). Figure 1.4 shows the variation in Nothern (black) and Southern (blue) hemispheric polar fields for the last 4 cycles. From Figure 1.4, it can be seen the asymmetry in the polar field of the Sun and variation in the

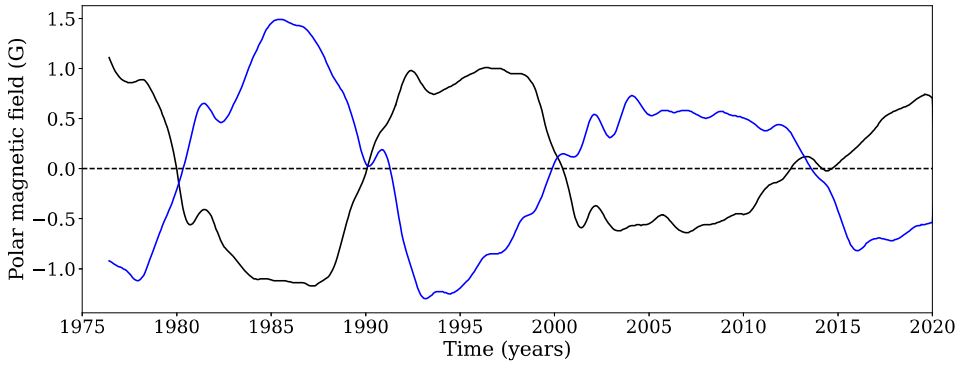

Fig. 1.4 Time series plot of the polar field of the Sun for northern (black) and southern (blue) hemispheres. We have used Gaussian smoothing filter (Hathaway et al., 2002a) with FWHM = 6 months for smoothing the data. This field is computed by averaging the radial field (derived from the measured line-of-sight component) from 55° to the poles. To remove the yearly geometric projection effect, a 20 nHz low pass filter has been used during the recording of the data. (*Source: Wilcox Solar Observatory, http://wso.stanford.edu/Polar.html*).

polar field reversal timing in both hemispheres. Furthermore, there is evidence of possible triple reversals of the polar field in the Sun (Makarov et al., 1983; Mordvinov et al., 2022). This phenomenon is believed to be caused by a high abundance of anti-Hale and non-Joy active regions (ARs) at a time. For details, see Figure 1.5 for solar cycle and polar field variation together and magnetic surges due to non-Joy and anti-Hale ARs.

The Sun's polar field plays a central role in understanding global solar magnetism and exerts a dominant influence over the heliosphere, akin to the solar cycle. Also, it is well-known that the generation of the polar magnetic field stems from the decay and dispersal of active regions (e.g., sunspots) that emerge in the lower latitudes and reverses the previous cycle polar field of that hemisphere. This polar field goes towards the base of the solar convection zone (SCZ) with the help of meridional flow, where due to differential rotation, this field becomes amplified and forms the toroidal field. Due to magnetic buoyancy, the toroidal field emerges on the solar surface as sunspots. Hence, Sun's polar field is

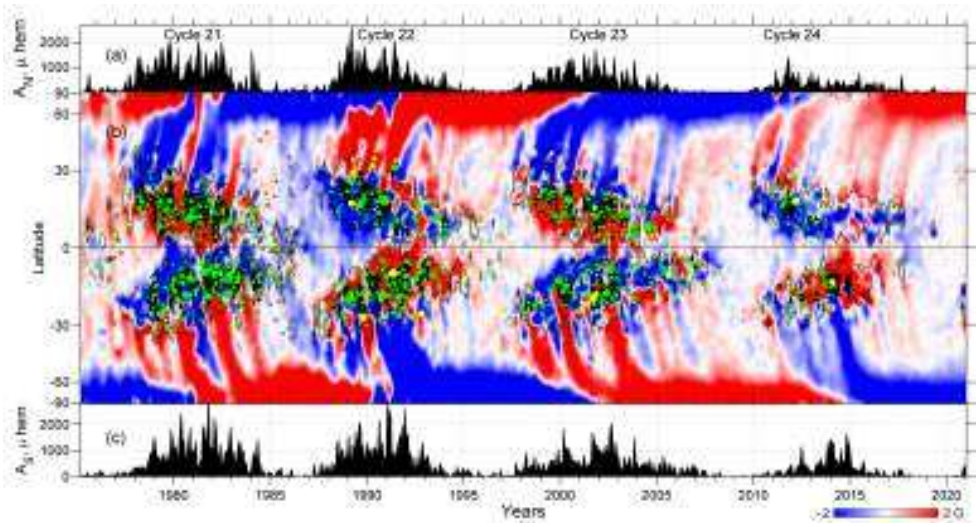

Fig. 1.5 Time-latitude distribution of the longitudinal average radial field on the solar surface. This image illustrates the polarity reversals, the generation of the poloidal field from the decay of active regions at low latitudes, and the drift of the field towards the polar region. Black contours represent the locations of high activity regions (sunspot band). Green and yellow points represent the non-Joy and anti-Hale active regions (ARs). (*Image courtesy: Mordvinov et al. (2022)).*

an essential component of the solar dynamo and plays a crucial role in the long-term sustenance of solar magnetism (see details in §1.4).

The number of sunspots increases and decreases with time on the solar surface. The variation of the sunspot number follows a cyclic pattern known as the Schwabe cycle (1844) or solar cycle, with an average period of 11 years (see Figure 1.6). The length of the cycle can vary irregularly from 9 years to 14 years (Hathaway, 2015). Besides 11 years cyclicity, the solar cycle exhibits some other characteristic features. i) The solar cycle possesses two phases known as solar maximum and solar minimum. The solar minimum corresponds to the period of low solar activity, characterized by the low number of sunspots observed on the Sun's surface. Conversely, the solar maximum represents the period of high solar activity, marked by the high number of sunspots observed during the solar cycle. ii) The amplitude of the solar cycle varies irregularly. A major focus of this thesis is to explore the cause of these irregular features of the solar cycle. iii) The solar cycle exhibits

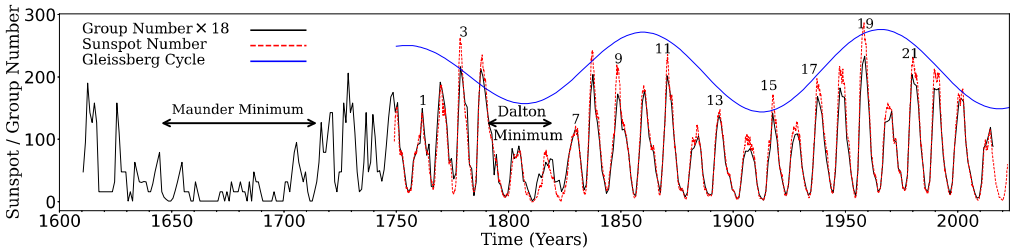

Fig. 1.6 Temporal variation of monthly mean sunspot number (ISN V2.0) smoothed using a Gaussian filter of FWHM = 7 months (red dashed curve), available since 1749, and the yearly mean group sunspot number (black curve) available during 1610–2015. Note that the group sunspot number is scaled by a factor of 18 to bring it to the scale of the sunspot number. The blue curve is the Gleissberg cycle, with a time period of 98 years. Cycle numbers for which the Gnevyshev–Ohl rule (Even–Odd rule) is obeyed are shown by indicating the number on the odd cycles. (*Source: WDC–SILSO, Royal Observatory of Belgium, Brussels, https://www.sidc.be/SILSO/datafiles, Image courtesy: Karak (2023)).*

an asymmetric shape with respect to its maximum; it takes less time to rise than to decline (Waldmeier, 1935). iv) Also, observations suggest the presence of double peaks (also called Gnevyshev Gaps) in most of the cycles (Karak et al., 2018; Takalo, 2023). The occurrence of double peaks in the solar cycle has primarily been observed in weak solar cycles. The double peaks phenomenon, in which two distinct peaks of solar activity occur within a single cycle, adds an additional layer of complexity to our understanding of solar magnetic field variability. v) In Figure 1.6, we also observe an extended period (during 1645–1715) when the sunspot number went to a low value which is popularly known as the Maunder minimum (Eddy, 1976). Another episode of about two cycles after 1800, when the sunspot number was relatively low, is known as the Dalton Minimum. In contrast to these grand minima, the sunspot number during the 20^{th} century was much higher and is known as the Modern grand maximum (Solanki et al., 2004). The reconstructed data over the millennial timescale also show the existence of grand minima and grand maxima (Biswas et al., 2023b; Usoskin, 2023). Additionally, long-term variation and modulation with timescale beyond 11 years have been observed in the solar cycle. The Gleissberg

cycle is one such example of this long-term variability. Thus, this suggests a possibility of memory in the solar magnetic cycle.

1.2 Proxies of Solar Magnetism

Various direct and indirect proxies of solar activity are utilized to study solar magnetism. These proxies can be classified into two types: physically measurable quantities and synthetic proxies, generated through algorithms using observed data. The usual key indicator of solar activity is the International Sunspot Number (ISN). The length of available direct observed sunspot number records is about 400 years. First Wolf (1848) started a proper catalog of sunspots on daily basis observations, which are known as Wolf sunspot number or Zürich sunspot number (R_z) defined by $R_z = k(10G + N)$, where k is the correction factor (observer-dependent), G is the number of identified sunspot groups, and N is the individual sunspots observed. This sunspot number data is most reliable from the Wolf time, and before the Wolf, it is far less reliable. The other proxy of solar magnetism is the sunspot area. In fact, sunspot areas are considered to be more physical measures of solar activity than sunspot numbers because the area represents the amount of magnetic flux emerges on the surface. The sunspot area data can be obtained from Royal Observatory, Greenwich (RGO) which is recorded since 1874 (https://solarscience.msfc.nasa.gov/greenwch.shtml).

Besides sunspot number and sunspot area, 10.7 cm solar radio flux, the geomagnetic activity, total solar irradiance (TSI), flares and CMEs, cosmic rays, nitrate in polar ice, and radioisotopes in tree rings and ice cores which can be used as the proxy of solar activity and thus solar magnetism (Traversi et al., 2012; Usoskin, 2023). The flux of galactic cosmic rays is modulated by the solar cycle. The galactic cosmic rays consist of high-energy electrons and bare nuclei. Due to positively charged nuclei, cascading showers of particles in Earth's upper atmosphere produce that can be measured by neutron monitors. With the

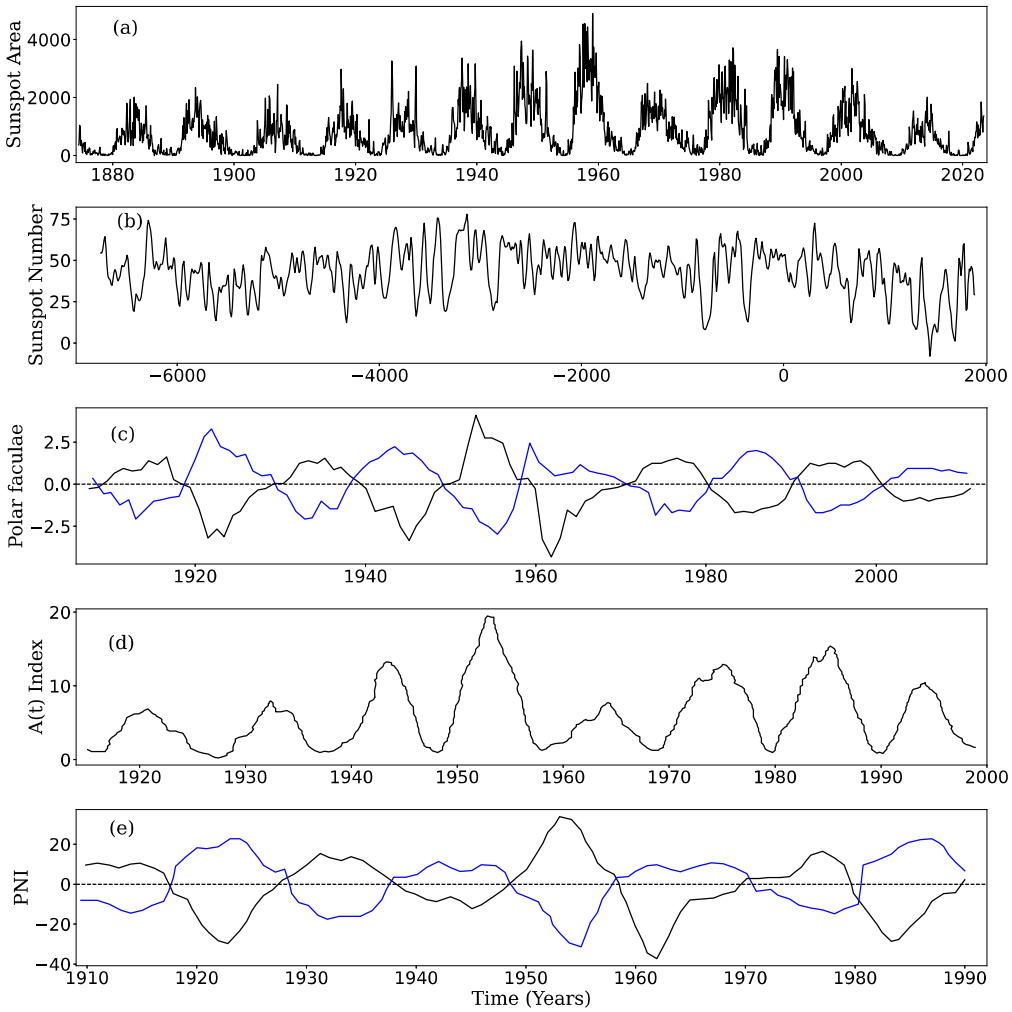

Fig. 1.7 Time series of different proxies of solar magnetism. (a) Sunspot area. (b) Sunspot number reconstructed from radioisotopes. (c) Hemispheric polar faculae count. (d) $A(t)$ index. (e) Hemispheric Polar Network Index (PNI).

increase in solar activity, the neutron counts fall. The cause is that at the time of high solar activity, magnetic structures are carried outward by the solar wind. These structures scatter incoming cosmic rays and reduce their flux in the inner solar system and heliosphere. Radioisotopes ^{14}C and ^{10}Be are used as the solar magnetic proxy produced in the Earth's stratosphere by galactic cosmic rays. ^{14}C is absorbed by trees, where it is stored in the form of annual growth rings, while ^{10}Be gets oxidized and becomes attached to aerosols that can precipitate in snow and are deposited in annual layers of the ice. The abundances of these isotopes govern by the galactic cosmic rays, modulated by the solar magnetic cycle (Usoskin, 2023). There are many other indices for measuring the solar magnetic field, such as the Magnetic Plage Solar Index (MPSI) and the Mount Wilson Sunspot Index (MWSI), Ca II K, H_α, Mg II K, EUV, polar network index (PNI), and polar faculae counts (Chatzistergos et al., 2022; Mordvinov et al., 2020; Muñoz-Jaramillo et al., 2012; Priyal et al., 2014; Sheeley, 1991; Xiang et al., 2014; de Haro Barbás et al., 2021). Figure 1.7 represents the temporal variation of some popular proxies of the solar magnetic field.

Furthermore, the auroral activity is also an indicator of solar activity, which is observed near Earth's polar regions. At the time of higher solar activity, the occurrence frequency of auroral events increases, and in lower activity, it gradually decreases. Sometimes, the solar activity is so high that the aurora is observed even in the lower latitudes. Recently Ladakh's (India) Hanle observatory captured a very rare aurora lights on April 23–24, 2023.

1.3 Prediction of Solar Activity and its Necessity

Solar activity is associated with its magnetic field. It has been observed that solar activity varies irregularly due to irregular variations in the Sun's magnetic field. The best representation of the random nature of solar activity is reflected by the observed sunspot numbers on the solar surface, which are the basis for the solar cycle. Figure 1.6 shows the irregular

variation of the solar cycle. The grand minima (Maunder minimum) and grand maxima are well-known examples of extreme variability in the Sun's magnetic field (Biswas et al., 2023b; Norton et al., 2023).

During periods of high solar activity, the occurrence of energetic events such as solar flares, coronal mass ejections (CMEs), and jets, is increased; see Figure 1.8, which shows the correlation of the occurrence frequency of solar flares with the solar cycle. These energetic events cause the release of a significant amount of energy and magnetic field into space, which causes space weather and disturbance in the Earth's magnetosphere and ionosphere (Temmer, 2021; Verdell, 2021). Due to these extreme and irregular solar activities, astronauts in space are subject to potentially lethal radiation dosages. Furthermore, these events can disrupt satellite communication and its operation in space, GPS navigation systems, power grids, gas pipelines, aircraft navigation, and Earth's technological infrastructure (Khodairy et al., 2020). Recently, SpaceX Starlink lost 38 satellites due to enhanced neutral density in the thermosphere associated with a geomagnetic storm (Fang et al., 2022). The cause of this is that the minor to moderate geomagnetic storm is sufficient to create 50%–125% density enhancement at altitudes ranging between 200 to 400 km. Thus geomagnetic storm (associated with solar activity) leads the thermospheric expansion and increases the satellite drag. There is also evidence that the solar activity affects human health. Zilli Vieira et al. (2019) reported that disturbance in geomagnetic activity enhances the risk of total and cardiovascular mortality.

Therefore, solar activity (associated with the solar cycle) prediction is essential for space weather forecasting, satellite operations, long-term space missions, climate studies, and advancing scientific knowledge of the Sun. It enables better preparedness, optimization of resources, and mitigation strategies to protect space assets and technological infrastructure and enhance our understanding of the dynamic magnetic field. The scientific community has developed several methods to predict solar cycle variability (Petrovay,

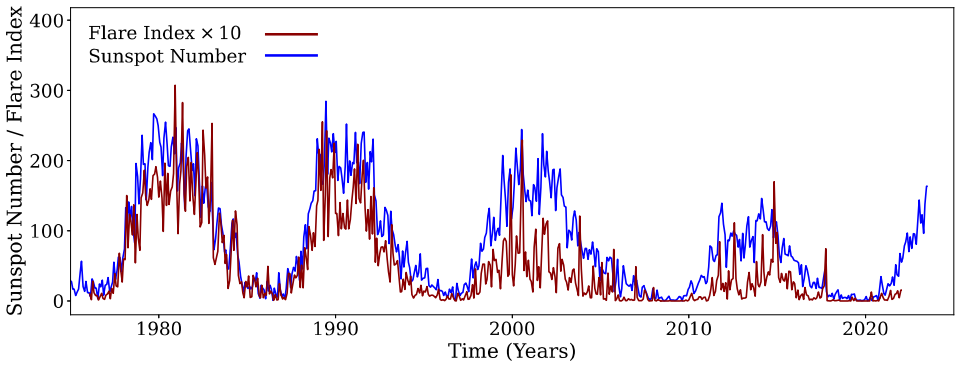

Fig. 1.8 Temporal variation of monthly mean sunspot number (ISN V2.0) and monthly mean solar flare index. Note that the flare index is scaled by a factor of 10 to bring it to the scale of the sunspot number. (*Source: WDC–SILSO, Royal Observatory of Belgium, Brussels, https://www.sidc.be/SILSO/datafiles, and Kandilli Observatory, Istanbul, Turkey, https://www.ngdc.noaa.gov/stp/space-weather/solar-data/solar-features/solar-flares/index/*).

2020). The most used method is the precursor in which some proxy of the solar magnetic field of past time is used to predict the next cycle variability. There are statistical methods also to predict solar activity, like extrapolation of time series. The model-based predictions (mainly using surface flux transport and dynamo model) are the new way to predict solar activity using different indicators of the solar magnetic field. A major portion of this thesis is dedicated to the solar cycle prediction, which will be discussed in Chapters 3–4.

1.4 Origin of Solar Magnetism

We have seen many different observational features of the solar magnetic field. Now, we shall try to develop a theoretical understanding of the generation and evolution of this magnetic field, i.e., the dynamo process. The recent development of crucial disciplines in physics, Magnetohydrodynamics, Helioseismology, and Magnetoconvection played a pivotal role in elucidating numerous observational features pertaining to the Sun's magnetic fields. Hence, we will present the basics of dynamo theory utilizing a single fluid descrip-

tion of the plasma and its interaction with the magnetic field using magnetohydrodynamics (MHD).

1.4.1 Basics of Magnetohydrodynamics

Magnetohydrodynamics (MHD) is an important discipline of physics that studies plasma dynamics coupled with the magnetic field. Indeed, magnetohydrodynamics (MHD) can be applied under certain specific circumstances. In the application of MHD, plasma is treated as a single fluid, and the length scales of the system should be larger than the Debye length, while the time scales should be larger than the inverse of the plasma frequency. Furthermore, while applying MHD to plasma dynamics, it is crucial to consider the non-relativistic approximation. These approximations allow MHD to effectively describe the behavior of the plasma in the solar and stellar CZ. The basic equations that govern the MHD are the following.

$$\frac{\partial \rho}{\partial t} + \nabla \cdot (\rho \boldsymbol{v}) = 0, \tag{1.1}$$

$$\frac{\partial \boldsymbol{v}}{\partial t} + (\boldsymbol{v} \cdot \nabla)\boldsymbol{v} = \boldsymbol{F} - \frac{1}{\rho}\nabla p + \frac{1}{\rho c}\boldsymbol{J} \times \boldsymbol{B} + \nu \nabla^2 \boldsymbol{v}, \tag{1.2}$$

$$\frac{\partial \boldsymbol{B}}{\partial t} = \nabla \times (\boldsymbol{v} \times \boldsymbol{B}) + \lambda \nabla^2 \boldsymbol{B}, \tag{1.3}$$

The equation (1.1) is the equation of continuity and equation (1.2) is the Navier-Stokes equation same as in the hydrodynamics case but only differs by the presence of magnetic force. For a non-relativistic plasma, the Navier-Stokes equation can be rearranged using the relation $\nabla \times \boldsymbol{B} = \frac{4\pi}{c}\boldsymbol{J}$, where $\boldsymbol{B}$ is the magnetic field and $\boldsymbol{J}$ is the current density. The magnetic force term then becomes $\frac{1}{4\pi\rho}(\nabla \times \boldsymbol{B}) \times \boldsymbol{B}$, and the equation can be written as:

$$\frac{\partial \boldsymbol{v}}{\partial t} + (\boldsymbol{v}\cdot\nabla)\boldsymbol{v} = \boldsymbol{F} - \frac{1}{\rho}\nabla(p + \frac{B^2}{8\pi}) + \frac{(\boldsymbol{B}\cdot\nabla)\boldsymbol{B}}{4\pi\rho} + \nu\nabla^2\boldsymbol{v} \tag{1.4}$$

where $\boldsymbol{F}$ represents the resultant body force consisting of, for example, gravity and Coriolis forces. From equation (1.4), it is evident that the magnetic force introduces a magnetic pressure of $\frac{B^2}{8\pi}$.

Equation (1.3) is the fundamental equation of the MHD and is known as the induction equation that determines the dynamical behavior of the magnetic field in the plasma. In addition to Equation (1.3), it is necessary to satisfy the divergence-free equation $\nabla\cdot\boldsymbol{B} = 0$. The parameters $\lambda = \frac{c^2}{4\pi\sigma}$ is the magnetic diffusivity and ν is the kinematic viscosity. The other notations have their usual meanings.

Equation (1.3) has two terms on the right side. If we consider B is the typical magnetic field, V is the typical velocity, and L is the typical length scale of the system, then the ratio of the first term to the second is known as the Reynolds number. This dimensionless quantity is defined as $R_M = \frac{LV}{\lambda}$. It is evident that R_M is directly proportional to the size of the system, and thus, for the astrophysical systems, it is much large ($R_M >> 1$). Hence, for astrophysical systems, the induction equation can be written as:

$$\frac{\partial \boldsymbol{B}}{\partial t} \approx \nabla\times(\boldsymbol{v}\times\boldsymbol{B})$$

Physically, the consequence of this equation is that the magnetic flux is frozen in the plasma and moves with plasma flows. This result is often called Alfvén's theorem of flux freezing and was first pointed out by Alfvén (1943). This theorem provides valuable insights into the generation and evolution of magnetic fields in various astrophysical systems, including Sun and Sun-like stars.

1.4.2 Magnetoconvection

Like magnetohydrodynamics (MHD), magnetoconvection plays an important role in understanding the magnetic behavior in astrophysical systems. Magnetoconvection occurs within the solar convection zone (SCZ), which is believed to be the birthplace of the solar magnetic field. Magnetoconvection is similar to thermal convection; however, it occurs in the presence of an imposed magnetic field within the plasma. In their seminal work, Thomson (1951) and Chandrasekhar (1952) conducted a rigorous analysis by perturbing the magnetohydrodynamic (MHD) equations to determine the conditions under which a magnetofluid becomes unstable for convection. They revealed that the presence of a strong magnetic field enhances the stability of the magnetofluid against convection. This can be explained by magnetic tension, which provides a physical explanation for the observed behavior. Further, Chandrasekhar (1961) demonstrated that when the magnetic field is stronger, it is harder to initiate convection. Understanding this result physically is not difficult because convection distorts magnetic field lines, and convective motions are opposed by magnetic tension. Therefore we need a steeper temperature gradient to drive the convection when a strong magnetic field is present. To understand the nature of magnetoconvection, the first impressive numerical simulations were carried out by Weiss (1981) using full non-linear MHD equations and showed that the magnetic fields are excluded from the regions of vigorous convection. The theory of magnetoconvection gives a crucial advancement to investigate the sunspots and granular and supergranular structures around the sunspots. Magnetoconvection effectively elucidates the reason behind the cooler temperatures observed in sunspots. Since sunspots have a strong magnetic field strength ($\sim$ 3000 G), the convection is inhibited by this magnetic field in the sunspot and thus lower temperature than surrounding. Note that magnetoconvection provides a basis for explaining certain features of sunspots and the behavior of magnetic fields associated with them, however, the origin of sunspots is still not fully understood.

1.4.3 Essentials of Solar Dynamo

It is well-established that the magnetic field generation and its sustenance in astronomical objects are due to the dynamo process. Moreover, in our Sun it is also believed that the 11-year solar magnetic cycle and its variability are regulated by the dynamo process. Therefore, in this section, we shall try to understand the dynamo mechanism in the Sun.

The generation, evolution, and behavior of the magnetic field in the Sun and astrophysical bodies can be comprehended by solving the magnetohydrodynamic (MHD) equations (1.2) and (1.3) along with the appropriate equations of state, energy, and continuity using two fundamental approaches. The first is the kinematic dynamo model, where the velocity field is specified, and the dynamo equation becomes linear in the magnetic field, allowing for relatively straightforward solutions. In the kinematic approach, we invoke large-scale flows like differential rotation and meridional circulation in the induction equation from observations. In the second approach, we solved the full dynamical equations of MHD. Thus in this approach, the large-scale flows are naturally produced. However, solving full MHD equations is numerically challenging and requires huge computation power. Only in recent years, there has been some progress in this field achieved, although, some discrepancies are still there (Charbonneau, 2020). Therefore the kinematic approach is more accessible than the full MHD calculation. In the kinematic dynamo model, however, we need to model the small-scale turbulent flows using a suitable approach e.g., mean-field approach.

Mean field kinematic dynamo model

The mean-field kinematic dynamo models are the most popular descriptive dynamo models for the magnetic field generation in the Sun and stars. In this model velocity field is used constrained by the observations. Here we only discuss the mean-field dynamo model in brief.

The initial concept of solar magnetic field generation and evolution was demonstrated by Parker (1955b) in his work on turbulent dynamo theory. Parker suggested that the poloidal and toroidal components of the magnetic field continuously exchange with each other, like the kinetic and potential energy exchange in the simple harmonic oscillator, and make the solar cycle oscillatory in nature. The possible cause of this exchange is the Ω effect and turbulent α effect.

After Parker's idea, Steenbeck et al. (1966) developed a rigorous mathematical formulation of Parker's turbulent dynamo theory. In addressing turbulence within the CZ, Steenbeck & Krause (1969) undertook an ensemble approach to deal with statistical properties and developed mean-field dynamo theory. In mean field theory, the velocity field and magnetic field are considered as the sum of mean and fluctuating components in the turbulent system and expressed as,

$$\boldsymbol{v} = \overline{\boldsymbol{v}} + \boldsymbol{v'}, \qquad \boldsymbol{B} = \overline{\boldsymbol{B}} + \boldsymbol{B'}, \tag{1.5}$$

with $\overline{\boldsymbol{v'}} = 0$ and $\overline{\boldsymbol{B'}} = 0$. Substituting these values in the induction equation(1.3) and taking the ensemble average, the induction equation is modified as,

$$\frac{\partial \overline{\boldsymbol{B}}}{\partial t} = \nabla \times (\overline{\boldsymbol{v}} \times \overline{\boldsymbol{B}}) + \nabla \times (\alpha \overline{\boldsymbol{B}}) + (\lambda + \eta)\nabla^2 \overline{\boldsymbol{B}}, \tag{1.6}$$

where $\alpha = -\frac{1}{3}\overline{\boldsymbol{v'} \cdot (\nabla \times \boldsymbol{v'})}\tau$, and $\eta = \frac{1}{3}\overline{\boldsymbol{v'} \cdot \boldsymbol{v'}}\tau$. $\boldsymbol{v'}$ and $\boldsymbol{B'}$ are the fluctuating components of velocity and magnetic field, respectively, and τ is the correlation time of the turbulence. η is the turbulent diffusivity and α is the helical turbulence which mimics the poloidal field generation coefficient in the dynamo model. λ is the molecular diffusivity which is negligible than turbulent diffusivity. Therefore, while solving the mean field equation, we neglect the molecular diffusivity.

After mathematical formalism, Steenbeck & Krause (1969) have solved the mean field equation (1.6) for Sun in spherical coordinates assuming with angular velocity $\boldsymbol{v}_\phi(r,\theta) = \Omega r \sin\theta\hat{\phi}$. They were able to reproduce the observed butterfly diagram from theoretical and numerical analysis (Steenbeck & Krause, 1969). The shape of the butterfly diagram suggests that the deep-seated toroidal field migrates toward the equator as the cycle progresses. In the mean-field dynamo, the dynamo waves propagation depends upon the combination of helical turbulence and differential rotation and follows the Parker-Yoshimura sign rule (In the northern hemisphere; $\alpha\frac{\partial\Omega}{\partial r} < 0$, dynamo wave propagate towards the equator and if $\alpha\frac{\partial\Omega}{\partial r} > 0$, dynamo wave propagate towards the poles.) (Parker, 1975; Yoshimura, 1975).

Note that observations of the Sun's large-scale magnetic field (shape of the solar corona, butterfly diagram of sunspots and magnetic field, and Hale's polarity law) suggest that it is axisymmetric about the rotation axis of the Sun and anti-symmetric about the equator. Therefore Sun's magnetic field can be written as,

$$\boldsymbol{B} = B_\phi(r,\theta,t)\hat{\phi} + \nabla\times\left[A(r,\theta,t)\hat{\phi}\right], \tag{1.7}$$

where,

$$\boldsymbol{B}_p = B_r\hat{r} + B_\theta\hat{\theta} = \nabla\times\left[A(r,\theta,t)\hat{\phi}\right],$$

where A is the magnetic vector potential. The poloidal component (B_p) and the toroidal component (B_ϕ) lie in the (r, θ) plane and in the azimuthal direction, respectively. The velocity field of the Sun is constrained by observations in this model. Hence, the velocity field can be considered as the combination of meridional flow and azimuthal flow such that, $\boldsymbol{v} = \boldsymbol{v_p}(r,\theta) + \boldsymbol{v}_\phi(r,\theta)$, and

$$\boldsymbol{v} = \frac{1}{\rho}\nabla\times\left[\psi(r,\theta)\hat{\phi}\right] + \Omega r\sin\theta\hat{\phi} \tag{1.8}$$

In this equation, the meridional flow is coming from stream function ψ, and azimuthal flow is coming from angular velocity Ω.

Since realistic dynamo operates in 3D, however, solving the dynamo in 2D, we consider the axisymmetric formulation of magnetic field and velocity field, and it resembles a crude approximation of the realistic dynamo in 2D. In the kinematic dynamo model approach with axisymmetric fields, solving mean-field equation (1.6) with (1.7) and (1.8) gives the evolution equations of poloidal and toroidal fields, which can be written as,

$$\frac{\partial A}{\partial t} + \frac{1}{s}(\mathbf{v}\cdot\nabla)(sA) = \eta_p\left(\nabla^2 - \frac{1}{s^2}\right)A + S_\alpha, \tag{1.9}$$

$$\frac{\partial B}{\partial t} + \frac{1}{r}\left[\frac{\partial}{\partial r}(rv_rB) + \frac{\partial}{\partial\theta}(v_\theta B)\right] = \eta_t\left(\nabla^2 - \frac{1}{s^2}\right)B + s(\mathbf{B}_p.\nabla)\Omega + \frac{1}{r}\frac{d\eta_t}{dr}\frac{\partial B}{\partial r}, \tag{1.10}$$

where s= $rsin\theta$ and $\boldsymbol{v}$ is the meridional circulation in (r,θ) plane. $S_\alpha = \alpha B$ and α is the coefficient of the poloidal field generation coefficient. Most of the previous models used the turbulent α effect as the poloidal field generation source, while in today's perspective, the alternative source of poloidal field generation is the Babcock–Leighton mechanism, which is discussed later.

Magnetic Buoyancy

The concept of magnetic buoyancy was introduced by Parker (1955b) to explain the formation of bipolar sunspots on the solar surface. Magnetic buoyancy is a crucial process which governs the rise of toroidal flux tube from the bottom of the convection zone to the surface (see Figure 1.9). Inside the convection zone it is believed that the magnetic field exists in the form of flux tubes, which are concentrations of magnetic field embedded within the plasma Choudhuri (2003). Now we consider an isolated magnetic flux tube

of toroidal flux inside the Sun's CZ . For a magnetic flux tube in hydrostatic equilibrium with the surrounding medium, if p_m is the tube's interior magnetic pressure, p_i is the fluid pressure inside the tube, and p_e is fluid pressure of the surrounding then,

$$p_e = p_i + p_m \tag{1.11}$$

where, $p_m = \frac{B^2}{8\pi}$ and equation becomes

$$p_e = p_i + \frac{B^2}{8\pi} \tag{1.12}$$

From equation (1.12), it is evident that $p_e > p_i$, and this usually, but not always, implies that the external density ρ_e is greater than the internal density ρ_i. When the temperature inside and outside the flux tube are equal, the flux tube will not be in mechanical equilibrium and will experience a buoyant force. Since astronomical bodies have high R_M, the magnetic field is frozen in the lighter fluid (Alfvén's theorem of flux freezing). As a result, the toroidal magnetic flux tube rises against the gravitational field and forms bipolar sunspots on the surface (see Figure 1.9(b)).

All numerical analyses in this thesis have been done in a 2D axisymmetric dynamo model and a 3D model. The incorporation of magnetic buoyancy into a 2D axisymmetric model poses challenges due to its inherent 3D nature. As a result, some crude approximations are often employed to include this phenomenon in the 2D axisymmetric dynamo model. Therefore different models use different methods to incorporate magnetic buoyancy (Dikpati & Charbonneau, 1999; Jouve et al., 2010a; Muñoz-Jaramillo et al., 2010). In the 2D model, an approach to incorporate magnetic buoyancy has been adopted as follows: (i) At regular time intervals (every 8.8×10^5 seconds), we search the latitudes above the base of the SCZ situated at $r = 0.71 R_\odot$ to identify regions where the toroidal field surpasses a critical value of $B_c = 10^5 G$. (ii) Then we reduce the toroidal field of an amount of $0.5B$

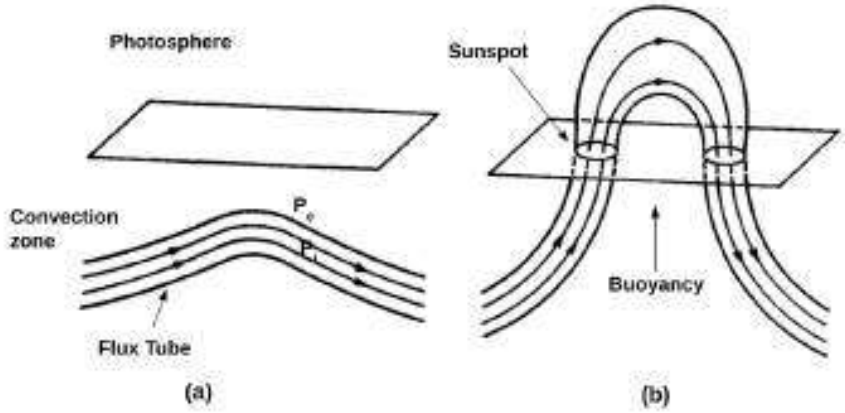

Fig. 1.9 The sketch of the magnetic buoyancy of a flux tube. (a) A nearly horizontal flux tube in the convection zone. (b) The flux tube after its upper part has risen through the solar surface due to magnetic buoyancy. The sketch is inspired by Choudhuri (1998).

and we add an equal amount of field on the solar surface at the corresponding latitudes . On the other hand, in the 3D model, the buoyancy effect is treated using a SpotMaker algorithm (see Chapter 2.2).

Meridional Circulation

Meridional circulation is one of the key components of the solar dynamo. Meridional circulation helps to migrate the surface magnetic field towards the poles from the active region's latitude and advects it from the surface to the bottom of the convection zone and towards the equator. Previous studies suggest that meridional circulation can significantly modulate the size and timing of the solar cycle through its impact on the Sun's polar magnetic fields. Thus it plays a crucial role in solar cycle variability (Biswas et al., 2023a; Hathaway & Upton, 2014).

Meridional circulation is well measured and observed on the solar surface using various techniques however, the equatorward return flow still lacks observational supports. Nevertheless, by applying the mass conservation principle, it is possible to construct a reasonable profile of the meridional circulation using its observed value on the surface.

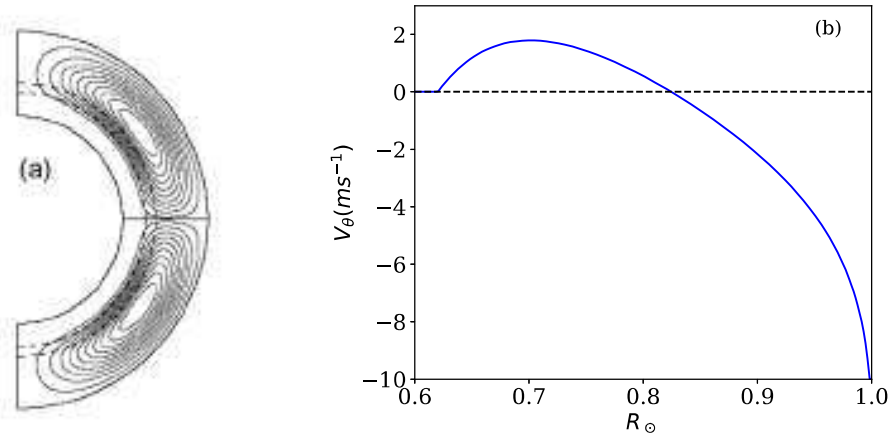

Fig. 1.10 (a) Meridional circulation streamlines used in the dynamo model. The dashed lines show the tachocline at the base of the convection zone (b) Variation of the latitudinal component of the meridional circulation at 45° latitude.

Although recent results support the view that the equatorward flow exists at the bottom of the convection zone (Gizon et al., 2020). The speed of meridional circulation estimated at the surface is ~ 20 m s^{-1} and base of the convection zone ~ 4 m s^{-1} at 45° latitude through observation and Helioseismology. In the last few years, some impressive numerical simulation of convection inside the rotating stars shows that turbulent stresses can drive large-scale flows (differential rotation and meridional circulation) (Featherstone & Miesch, 2015; Karak et al., 2015a); see Choudhuri (2021) review for details. Therefore, it is assumed that the streamlines of the meridional circulation would remain confined within the convection zone. In this thesis, we have considered the single-cell (in one hemisphere) meridional circulation spanning the whole of the convection zone consistent with the observations (Gizon et al., 2020; Rajaguru & Antia, 2015) (see Figure 1.10). To be consistent with observations, we have assumed the poleward flow near the surface and the equatorward flow at the bottom of the convection zone. We define the meridional circulation using a stream function ψ such that,

$$\rho \boldsymbol{v} = \nabla \times \left[\psi(r,\theta)\hat{\phi} \right], \tag{1.13}$$

where

$$\psi r \sin\theta = \psi_0 (r - R_p) \sin\left[\frac{\pi(r-R_p)}{(R_\odot - R_p)} \right] \{1 - e^{-r\beta_1 \theta^\varepsilon}\} \{1 - e^{-r\beta_2 \theta^\varepsilon}\} e^{((r-r_0)/\Gamma)^2}$$

and density stratification,

$$\rho = C(\frac{R_\odot}{r} - \gamma)^m$$

The parametric values are,

$\beta_1 = 1.36 \times 10^{-8}\ m^{-1}$, $\beta_2 = 1.3 \times 10^{-8}\ m^{-1}$, $\varepsilon = 2.0$, $r_0 = 0.1286 R_\odot$, $\Gamma = 3.025 \times 10^8\ m$, $\gamma = 0.95$, $m = 3/2$, $R_p = 0.635 R_\odot$.

Figure 1.10 (a) shows the meridional circulation stream lines and (b) shows the latitudinal component v_θ at mid-latitude 45° obtained from the above stream function, which has been used in our dynamo simulations.

Turbulent Diffusion

Turbulent diffusivity is an important component of the dynamo which plays a crucial role in the redistribution and transport of the magnetic field to the poles and maintains the solar dynamo activity. Considering mean field theory and first-order approximation, diffusivity can be defined as,

$$\eta = \frac{\tau}{3} \left\langle \boldsymbol{v^2} \right\rangle, \tag{1.14}$$

where $\boldsymbol{v}$ is the turbulent velocity field and τ is the eddy correlation time. Nevertheless, turbulent diffusivity is properly constrained throughout the CZ; however, observations and

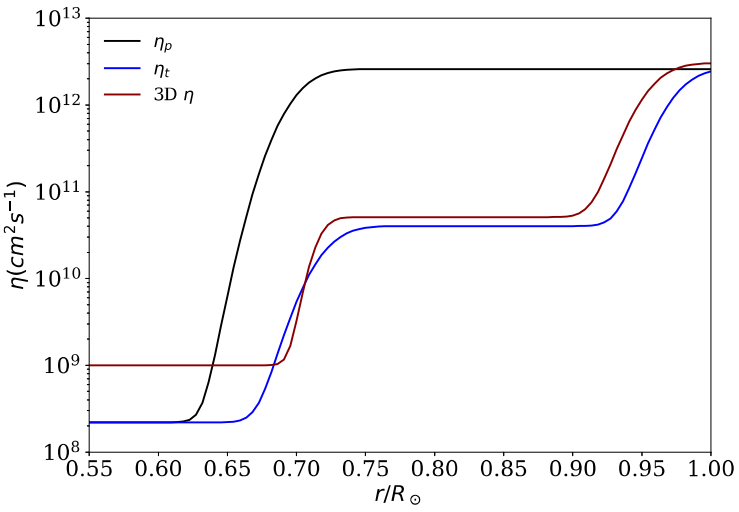

Fig. 1.11 Diffusivity profile for the solar dynamo. Blue and black curves show the variation of toroidal diffusivity and poloidal diffusivity in the 2D *Surya* dynamo model; however, the dark red curve shows the turbulent diffusivity in the 3D dynamo model with solar radius.

simulations suggest that the value of turbulent diffusivity near the surface is of the order of 10^{12} cm^2 s^{-1} (Chae et al., 2008).

The profile of turbulent diffusivity used in the dynamo model for this thesis is shown in Figure 1.11. In the 2D dynamo model, we use different values of diffusivity for the poloidal and toroidal components. The two values, namely η_p and η_t are comparable near the surface and below the surface η_p is greater than η_t. Some authors suggested significant quenching in the diffusivity due to the strong magnetic field in the CZ, i.e., the toroidal field (Guerrero et al., 2009; Muñoz-Jaramillo et al., 2011). Since the poloidal field is weaker than the toroidal, η_p should be larger than the η_t. The value of η_p used in this model is close to the convective velocity in the CZ derived from the observed properties of flows (Miesch et al., 2012).

For the 3D dynamo model, we use the same value of η for poloidal and toroidal components, and for this, we use a two-step profile (see details in Chapter 2.2). It is evident that the theory of turbulent diffusion is not well understood. However, different

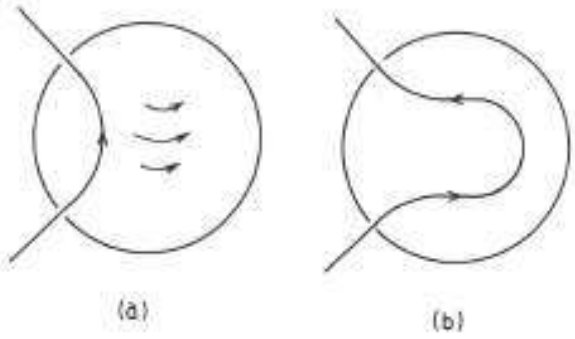

Fig. 1.12 The sketch of the generation of the toroidal field from the poloidal field in the solar convection zone (SCZ) due to differential rotation, i.e., Ω effect. (a) Initial poloidal field line. (b) Field line after stretches due to differential rotation in the Sun, *(Image courtesy: Choudhuri (1998)).*

profiles used in the dynamo model produce results that are qualitative agreement with the observations.

Generation of toroidal field (Ω effect)

The Sun exhibits differential rotation, with its equator rotating faster than the higher latitudes. This phenomenon has been extensively studied and well-mapped through helioseismology (Schou et al., 1998). Evidence suggests that within the solar convection zone (SCZ), the differential rotation varies with latitude and Sun's radius (Howe, 2009, 2020). In the solar dynamo, it is well-established that the poloidal magnetic field gives rise to the toroidal magnetic field. The differential rotation (Ω effect) acts to stretch the poloidal magnetic field in the ϕ direction and results in an amplification of the field strength (see Figure 1.12). Thus it gives the toroidal field. This toroidal field appears on the solar surface in the form of sunspots or BMRs due to magnetic buoyancy. Here we note that in the presence of magnetic diffusion, the poloidal field would undergo decay over time. Consequently, without a continuous supply of the poloidal field through some other means i.e., α effect, the generation of the toroidal field would eventually come to a halt.

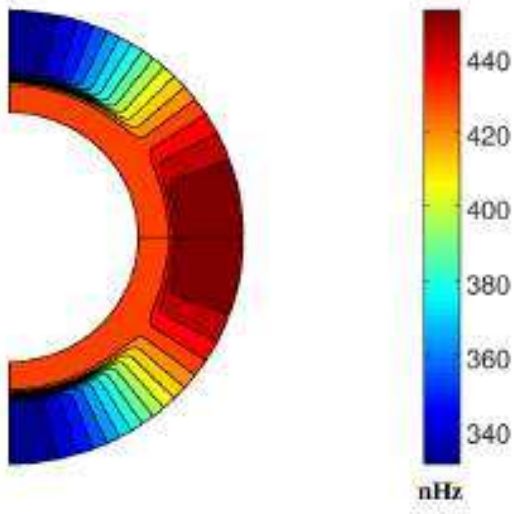

Fig. 1.13 Differential rotation profile from the model.

The analytical profile of differential rotation which has been used in our dynamo model and is shown in Figure 1.13 is guided by the helioseismic observations (Dikpati & Charbonneau, 1999; Schou et al., 1998). We have neglected the near-surface shear layer in our model, which has negligible effect in the generation of the toroidal field (Dikpati et al., 2002); however, see Karak & Cameron (2016) for the demonstration of its effect in shaping the equatorward migration of the toroidal field.

Generation of poloidal field

Due to the magnetic diffusivity of the Sun, the poloidal field decays, and eventually, the generation of the toroidal field will stop. However, in the Sun, we get an oscillatory nature of the magnetic field. To explain this, Parker (1955b) gave a crucial idea of poloidal magnetic field generation in the Sun. Since SCZ is highly turbulent and the toroidal magnetic field rises through this convection zone due to magnetic buoyancy, the Coriolis force introduces a helical twist on the rising plasma blobs. Thus due to Alfvén's flux

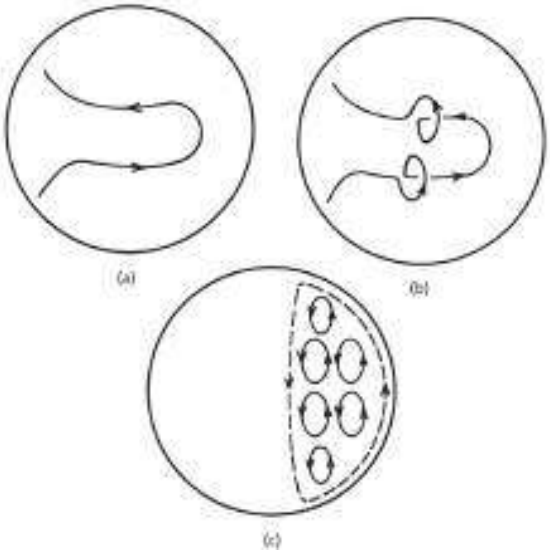

Fig. 1.14 The sketch of the different stages of the dynamo process. (a) Initial poloidal field line stretches due to Ω effect. (b) Twisting in the toroidal field lines due to helical turbulence. (c)Generation of the poloidal field from turbulent α effect, *(Image courtesy: (Choudhuri, 1998))*.

freezing concept, the magnetic field lines will be frozen in the plasma and twisted because of the helical turbulence.

This phenomenon occurs in a rotating frame of reference, resulting in vorticity with opposite senses in the two hemispheres. Consequently, the twisting of the toroidal magnetic field in the two hemispheres also exhibits opposite signs. As a result of this behavior, the projected magnetic loops in the poloidal plane would exhibit the same sense in both hemispheres (see Figure 1.14 (c)). Further, due to strong turbulent diffusion in the sun's cz, the cumulative effect of several loops give rise to a large-scale poloidal magnetic field as shown by the dashed line in Figure 1.14 (c). Thus due to helical turbulence, the poloidal field can be produced from the toroidal field and the process is known as the turbulent α effect or classical α effect. Therefore, toroidal field generation from the poloidal field by stretching (Ω effect), and the generation of the poloidal field from toroidal one i.e., α effect. Thus the magnetic cycle and dynamo sustain in the long term.

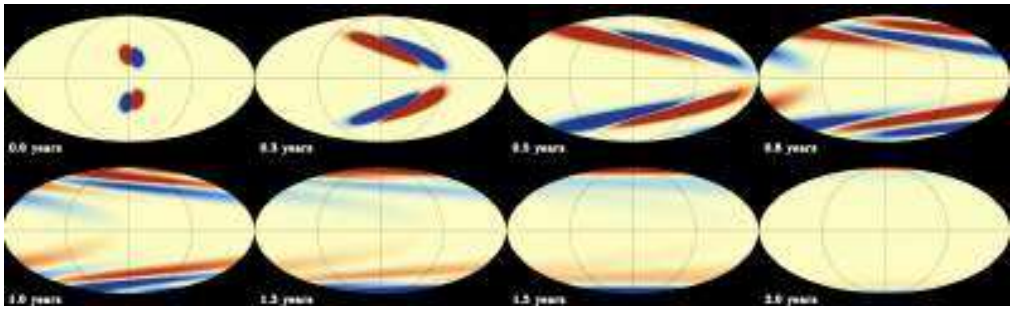

Fig. 1.15 Babcock–Leighton mechanism demonstration (for three years) through decay and dispersal of two BMRs deposited at 25° latitude symmetrically in both hemispheres. BMRs tilt assigned by Joy's law and weak poloidal field deposited at the poles after three years are shown, *(Image courtesy: (Karak, 2023))*.

However, after some time of the idea of turbulent dynamo theory, it has been realized that in the presence of a strong toroidal magnetic field (order of $\sim 10^5$ G), turbulent α effect would not be able to generate the poloidal field due to helical turbulence in the convection zone (Choudhuri & Gilman, 1987; D'Silva & Choudhuri, 1993). Therefore to complete the dynamo loop (toroidal to poloidal), authors adopted the Babcock (1961) and Leighton (1964, 1969) idea of poloidal field generation. This idea is popularly known as Babcock–Leighton α effect. The Babcock–Leighton process is clearly observed in the synoptic magnetograms and well produced in the Surface flux transport (SFT) model (Dasi-Espuig et al., 2010; Kitchatinov & Olemskoy, 2011; Lemerle et al., 2015b). In the Babcock–Leighton mechanism, the large-scale poloidal field is generated from the decay and dispersal of tilted active regions (sunspots or BMRs) near the surface. Figure 1.15 shows the generation of the large-scale poloidal field through decay and dispersal of tilted BMR ($\sim 14°$) in the Babcock–Leighton process for 3 years. Due to the tilt angle of ARs, the leading polarity is closer to the equator compared to the trailing polarity. As a result of this configuration, a considerable amount of magnetic flux of the leading polarity cancels out with the opposite polarity in the other hemisphere due to transequatorial cancellation. On the other hand, the trailing polarity flux tends to move towards the pole, where it cancels out the opposite polarity flux from the previous cycle and builds the poloidal field

for a new cycle (Babcock, 1959; Babcock & Livingston, 1958). We note that the poloidal field strength generated through Babcock–Leighton α effect mainly depends upon the average tilt angle of the ARs (sunspots). In this thesis, the poloidal field generation source is the Babcock–Leighton α effect in the dynamo model. Therefore, this type of dynamo is called the Babcock–Leighton dynamo.

1.4.4 Babcock–Leighton Dynamo Model for Solar Cycle

We have seen the important ingredients of the solar dynamo. Now I will discuss the observationally supported dynamo model, which is known as the Babcock–Leighton dynamo model (Babcock, 1961; Cameron & Schüssler, 2017b; Cameron et al., 2018; Leighton, 1964, 1969). In the Babcock–Leighton dynamo model, the poloidal field is produced near the surface at low latitudes through the Babcock–Leighton process and advected towards the high latitudes and further to the deep CZ with the help of meridional flow, where the Ω effect stretches the poloidal field to give rise to the toroidal field. Due to magnetic buoyancy, this toroidal field emerges on the solar surface in the form of BMRs (Parker, 1955a). See Figure 1.16 for Babcock–Leighton dynamo mechanism in a nutshell.

Equations (1.9) and (1.10) are the foundation of Babcock–Leighton dynamo. In equation (1.9), $S_\alpha = \alpha B$, where α describes the poloidal field generation from the toroidal field in the Babcock–Leighton type dynamo. Indeed, the Babcock–Leighton mechanism is a 3D process, and the depiction of it in the 2D axisymmetric dynamo model gives only a crude approximation of this process. To use Babcock–Leighton α mechanism in our 2D dynamo model, we have chosen the α in the following way:

$$\alpha = \frac{\alpha_0}{4}\cos\theta\left[1+\mathrm{erf}\left(\frac{r-0.95R_\odot}{0.025R_\odot}\right)\right]\times\left[1-\mathrm{erf}\left(\frac{r-R_\odot}{0.025R_\odot}\right)\right], \qquad (1.15)$$

where $R_\odot$ is the solar radius. We note that the Babcock–Leighton mechanism operates in the surface layer of the Sun (see Figure 1.17) and ensure that it is constrained with $0.95R_\odot < r < R_\odot$. Furthermore, in the Babcock–Leighton dynamo model, the poloidal field is generated through the Babcock–Leighton mechanism which depends on the tilt angle of ARs. Moreover, this tilt comes from the Coriolis force, which has a $\cos\theta$ dependency. Therefore, in α profile, to make it consistent with observation, we have taken $\cos\theta$. For dynamo saturation, we have used the nonlinear α quenching, and multiply in α by a factor, $\left[1+\left(\frac{B}{B_0}\right)^2\right]^{-1}$. Figure 1.17 shows the brief summary of Babcock–Leighton dynamo mechanism in the convection zone. In this type of dynamo, a strong toroidal field is generated on the base of the CZ, i.e., in the tachocline (green color). The strong toroidal field rises due to magnetic buoyancy (red arrows) and produces BMRs or ARs on the solar surface. However, the time scale of rising flux loops of the toroidal field and the subsequent emerging flux from the base of CZ is generally compared to be shorter than the cycle time period. Therefore, the Babcock–Leighton dynamo model typically does not explicitly include these process but rather incorporate a source term near the surface that mimics the deep-seated toroidal field in the convection zone (also see Figure 1.17) (Cameron & Schüssler, 2023; Charbonneau, 2020; Hazra et al., 2023). Due to the Babcock–Leighton mechanism, these ARs decay and disperse near the surface and produce the poloidal field. This process can be considered as a simple random walk on the solar surface and approximated as a diffusion process (Leighton, 1964). Thus to complete the dynamo loop, we should have some transport mechanism for magnetic flux transport to connect the two specially segregated regions of poloidal and toroidal fields. Observations and simulations suggest that meridional circulation, turbulent diffusivity, and turbulent magnetic pumping are these transport mechanisms.

After the specification of essential ingredients and parameters of the Babcock–Leighton solar dynamo, we can solve the equations (1.9) and (1.10). In this thesis for most of the

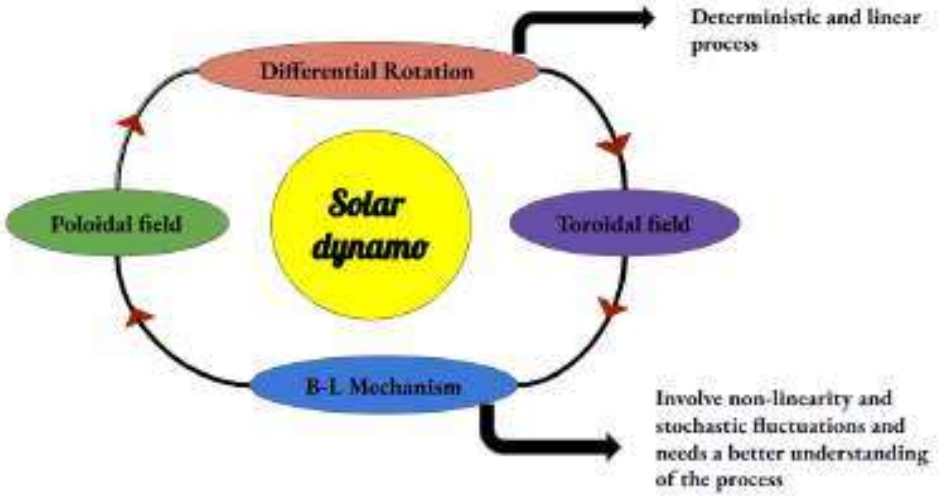

Fig. 1.16 Cartoon representation of the Babcock–Leighton dynamo loop.

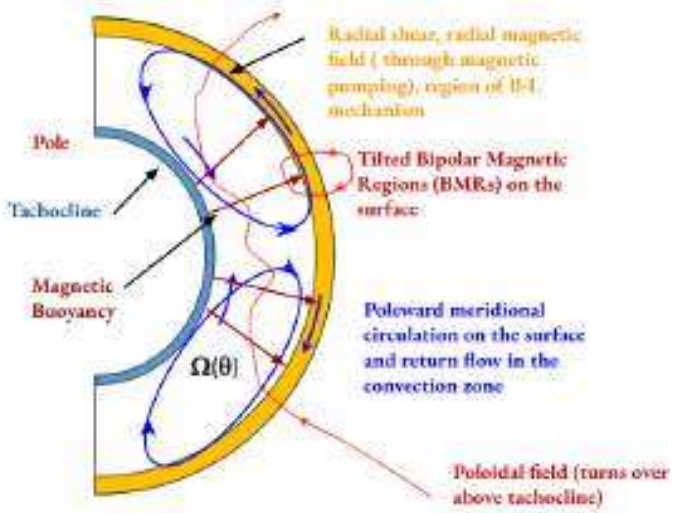

Fig. 1.17 The details of the Babcock–Leighton dynamo model in a meridional cut of the solar convection zone *(Image courtesy: (Cameron & Schüssler, 2023)).*

calculation, we carry out the following parameters in a meridional slab of $R_b = 0.55R_\odot < r < R_\odot$ and $0 < \theta < \pi$ with some boundary conditions: At the poles $A = 0$, $B = 0$, and $\theta = (0, \pi)$. The bottom boundary of the convection zone at $r = R_b = 0.55R_\odot$, assumption with perfect conductor. Therefore, at the bottom $A = 0$ and $B = 0$. This boundary condition is insensitive as long as it will be much below the meridional penetration depth. At the surface ($r = R_\odot$, toroidal field B should be zero and A should match a potential field satisfying the space free equation; $\left(\nabla^2 - \frac{1}{r^2 \sin^2\theta}\right) A = 0$. In most of the calculations, we have used 129×129 or 257×257 grid points to study the numerical calculation. This model is able to produce most of the features which are observed in the Sun.

In 3D dynamo model, to capture the Babcock–Leighton mechanism is more complex and we have discussed it in detail in Chapter 2.2. The 3D treatment of Babcock–Leighton mechanism makes the flux transport dynamo model more realistic and helps to capture the polar field and other observed phenomena in much more detail.